Research Article

Open Access Journal of
Biomedical Science
ISSN: 2690-487X

# Facile Synthesis of Chitosan Nanoparticle with Different Features and Histopathological Ultrastructural Study on The Effect of Its Bio-complex with Bovine Serum Albumin in Mice Liver

**Moataz M Rashad and Maged El-Kemary***

*Institute of Nanoscience & Nanotechnology, Kafrelsheikh University, Egypt*

## ABSTRACT

We have synthesized chitosan nanoparticles (CS-NPs) with different characteristics using ionic gelation method. Results showed that the synthesized CS-NPs with different concentrations of trisodium polyphosphate (TPP) are irregular - spherical shaped with narrow size distribution and high stability. The microporous chitosan was also synthesized with new features characterized with different techniques as SEM, EDX, FTIR and BET. The synthesized microporous chitosan has a surface area and pore volume of 245.571$m^2$/g and 0.155$cm^3$/g respectively. Its microporous surface is functionalized with carboxyl and amine groups. Histopathological and ultrastructural studies of mice liver were performed using optical and scanning electron microscopy (SEM) by intraperitoneal (IP) injection of male mice to evaluate toxicity of free and BSA-CS-NPs inside the body after three, six and nine days. However, no pathological or illness signs were observed in mice throughout the *in vivo* experiment with non-significant changes on body and relative weight of liver in compared to the negative control group. In addition, biochemical parameters exhibited a normal functionality of liver after BSA-CS-NPs administration. Accordingly, mild histopathological or ultrastructural alterations were observed in the liver of treated mice in all groups with respect with the negative controls. Activated Kupffer cells and leukocytes were observed due to the synergism of adjuvant effect of CS-NPs and antigenic peptides involved in BSA. Herein, we opened new direction for synthesis of different forms of CS-NPs and providing an obvious insight on histopathological and ultrastructural changes after administration of CS-NPs and its protein bio-complexes.

**KEYWORDS:** Ionic gelation; Chitosan nanoparticle; Microporous chitosan; Histopathology; Ultrastructure

**ABBREVIATIONS:** AST: Aspartate Transaminase; ALT: Alanine Transaminase; TPP: Trisodium Polyphosphate; BET: Brunauer-Emmett-Teller; BJH: Barrett-Joyner-Halenda; Scanning Electron Microscope: SEM; SPSS: Statistical Package for the Social Sciences; ANOVA: Analysis of Variance; TSC: Trisodium Citrate; TCDD: Tetra Chloro Dibenzo-p-Dioxin

## INTRODUCTION

Chitosan is a linear polysaccharide composed of a deacetylated unit (β-(1→4)-linked D-glucosamine) and acetylated one (N-acetyl-D-glucosamine). It is the most valuable and common derivative of chitin. Chitin represents the external exoskeleton of arthropods as insects and crustaceans, the radulae of mollusks, cephalopod beaks, and the scales of fish and Lissamphibia's [1,2]. Recently, Chitosan has been involved in several biomedical applications as drug delivery, gene therapy, tissue engineering, and wound healing, due to its unique chemical properties, mucoadhesivity, proper

**Quick Response Code:**

**Address for correspondence:** Maged El-Kemary, Institute of Nanoscience & Nanotechnology, Kafrelsheikh University, Egypt

**Received:** December 12, 2021 **Published:** February 22, 2022

**How to cite this article:** Moataz M R, Maged E K. Facile Synthesis of Chitosan Nanoparticle with Different Features and Histopathological Ultrastructural Study on The Effect of Its Bio-complex with Bovine Serum Albumin in Mice Liver. 2022- 4(1) OAJBS.ID.000402. **DOI:** 10.38125/OAJBS.000402

biocompatibility, biodegradability, and antibacterial properties. However, chitosan can be existed in many physical forms as nanoparticles, microparticles, membranes, nanofibers, sponges, gels, and scaffolds [3-5].

Nanoporous scaffolds are subdivided into microporous, mesoporous and macroporous depending on pore size. Microporous scaffolds have surface pores less than 2nm while mesoporous ones have pores of 2:50nm. Whereas macroporous scaffolds have surface pores with size exceeds 50nm [6]. Microporous chitosan can be used in drug/ vaccine delivery, catalysis, and water purification. It is well known that microporous chitosan microgel scaffold can also be convenient for localized surgical injections and regenerative medicine [7,8].

In addition, it has reported that microporous chitosan in combination with other substances as nano ZnO [9] nano Ag/ZnO, nanofibrin [10,11] and polyethylene glycol are used in different biomedical applications including antibacterial wound dressing, skin tissue regeneration and antibacterial drug delivery membranes [12].

In the past years, the synthesis of chitosan nanoparticles has been extensively considered [13], relatively less attention has been devoted to the synthesis of microporous chitosan. Herein, we provide overview on transforming nanochitosan into microporous chitosan via precipitation-step by trisodium citrate that provides good stability and large surface delivery platform for pharmaceutical purposes. Additionally, the synthesized microporous chitosan has been characterized by SEM, EDS, FTIR and BET techniques.

Due to their biocompatibility and biodegradability, protein-based nanostructures have a great interest in the field of nanomedicine as drug delivery, vaccine, biosensors, and imaging. These nanostructures can be existed either as protein nanoparticles or protein/nano-polymer complexes. Protein nanoparticles as albumin, gelatin and elastin can be synthesized by electrospray, desolation, emulsification and complex coacervation. Protein/ nano-polymers can be synthesized either by encapsulation or surface functionalization on nanostructured polymers as chitosan, polyvinyl alcohol, and cellulose. [14] Carrier proteins are one of the most important protein categories used in the field of vaccine industry due to its immunogenicity and biocompatibility inside the body. Also, they were used as antitumor, anti-inflammatory, [15] antimicrobial and immunotherapeutic agents [16,17]. Common carrier proteins are as keyhole limpet hemocyanin (KLH), ovalbumin (OVA), conalbumin (CONA) and human serum albumin (HSA) [18] as well as bovine serum albumin (BSA). [19] BSA is considered as a carrier protein that has some long antigenic peptides that was reported to be used to increase rhamnose and sTn antigen uptake for cancer vaccine development and in combination with rutin for the suppression of heme toxicity [20].

In our previous study, we developed a detailed protocol for *in vivo* toxicity evaluation of free and BSA-CS-NPs in terms of hematological, biochemical, spleen/ kidney histopathological observations and hypersensitivity [21]. The present study focuses on synthesis of different forms of CS-NPs that gives them the availability for the application in different fields of technology. Besides, we study the effect of the most convenient physiochemically synthesized free and BSA-CS-NPs in the liver functionality of albino male mice after IP administration for nine days that provides a complete insight about the safety and biocompatibility of CS-NPs to be used in the biomedical fields.

## EXPERIMENTAL

### Materials

Chitosan (Low Molecular Weight, 50 KDa, 90-95% deacetylation) was purchased from Oxford, Mumbai, India. Sodium tripolyphosphate (TPP) (Mw=367.86g/mol) and Trisodium citrate (Mw=294.1g/mol) was purchased from Sigma Aldrich. All reagents were of analytical grade and used as received. Double distilled water was used in the experiments.

### Methods

#### Synthesis of microporous chitosan

Chitosan (wt%) was prepared in glacial acetic acid of 1% concentration as a stock solution. Chitosan nanoparticles were synthesized by dropwise addition of 0.1mg/ml of sodium tripolyphosphate (TPP) drop by drop into chitosan acidic solution (0.1wt%) with a volume ratio (1:5, TPP:CS, v/v) under magnetic stirrer at room temperature for 1hr. Each 3ml of the synthesized chitosan nanoparticles solution was mixed with 1ml of trisodium citrate (1M). The produced precipitate was centrifuged at 6000 rpm for 15min and dried at 400C for 2hr and then the final product was obtained.

The physiochemical properties of the synthesized CS-NPs were studied using Brookhaven zeta-sizer (ZETAPALS, USA).

#### Effect of pH

3ml of synthesized CS-NPs solution was mixed with 1ml of trisodium citrate (1M). The formed precipitate was collected via centrifugation at 6000rpm for 15min and dried at 40°C for 2hrs. The specific surface areas, pore diameter and volume were determined by the adsorption isotherm of $N_2$ with Brunauer-Emmett-Teller (BET) and Adsorption Analysis. Pore size distributions were calculated from desorption branches of isotherms by the Barrett-Joyner-Halenda (BJH) method. Surface functionalization was investigated using FTIR technique and line/mapping - EDX analysis and morphology using SEM.

#### Synthesis of CS-NPs with BSA bio-complexes

1mg/ml of BSA was prepared in double distilled $H_2O$. BSA solution was added in a drop wise addition to CS-NPs solutions, in a volume ratio 1:1 (NP: BSA, v/v).

#### Characterization techniques

Morphology was observed by the scanning electron microscope (SEM, JEOL JSM-IT100). The dried sample of the precipitate and one drop of solutions was adhered on the conductive carbon tape placed on the copper stub. Then, the sample was sputtered coating with gold for 1 min. The measurements were performed at a voltage of 20KV and a current of 30A. Elemental analysis was performed using the silicon - drift EDS detector (energy resolution about 129 eV or better) with the analysis condition of WD 10mm and voltage 20KV. FT-IR analysis was performed using JASCO FT-IR Spectrometer (FT-IR 6800).

### *In vivo* experiment

#### Animals

4-6 weeks ago, Male albino mice (25 ± 5g) were used in this test. Animals were housed in polypropylene cages at room temperature for a 12hrs. light/ 12hrs. dark cycle. They were provided with a free access of water and a standard 17% proteinic diet.

### Treatment

After acclimation for a week, animals were randomly divided into six groups, ten mice per each. Mice were IP administrated with the corresponding treatments as described in Table 1 one time per day for nine day [21,22]. Blood and liver Samples were collected every 3rd day after sacrificing animals by decapitation. All experimental procedures were performed according to the approval of Institutional Animal Care protocol and Committee of Post- graduate Studies and Research at Kafrelsheikh University, Egypt.

**Table 1:** Mice groups with their corresponding treatment of the *in vivo* experiment.

| Group | Treatment |
|---|---|
| Negative control | Normal saline |
| BSA control | BSA (1mg/ml/Kg.b.w) |
| CS-NPs 1 control | CS-NPs (1mg/ml/Kg.b.w) |
| CS-NPs 2 control | CS-NPs (5mg/ml/Kg.b.w) |
| BSA-CS-NPs 1 | BSA-CS-NPs (mg/ml/Kg.b.w) |
| BSA-CS-NPs 2 | BSA-CS-NPs (5mg/ml/Kg.b.w) |

### Biochemical Analysis

Serum was isolated from the retro-orbital sinus vein of mice every 3rd day. Biochemical parameters determined were aspartate transaminase (AST) and alanine transaminase (ALT), albumin, globulin, albumin/globulin ratio using a biochemistry analyzer (Microlab 300, India).

### Histopathological Analysis

5µm sections of liver samples were fixed in 10% buffered formalin for 48h. Dehydration was performed in ascending concentrations of ethanol (50, 70, 95, 100 and 100%). Finally, samples were stained with Hematoxylin and Eosin protocols. All preparations were analyzed under a light microscope.

### Ultrastructural Analysis

1mm3 sections of liver samples were fixed in 2.5% buffered glutaraldehyde for 24 hrs. post-fixation was performed using 1% osmium tetroxide for 1hr. followed by a dehydration process in 50, 60, 70, 80, 90, 95, 100 and 100% ethanol concentrations. Finally, samples were dried in critical point dryer (Tousimis Autosamdri-815 Coater). The dried samples were adhered on stubs using an adhesive carbon tape and sputter coated with gold for 1min and the examination was performed using SEM (JEOL, JSM IT-100) at 20kV.

### Statistical analysis

Statistical analysis was performed with Statistical Package for the Social Sciences (SPSS) 20.0 versions and Excel software 2003 version. All results are calculated as the mean ± standard deviation of the mean. A value of $P<0.05$ was considered to be statistically significant. The statistical significance was calculated by one-way analysis of Variance (ANOVA) with Bonferroni's post-hoc comparison test. In case of non-homogeneous data, the significance was determined with the Mann-Whitney test and the Wallis - Kruskal test in case of abnormal distribution data.

## RESULTS AND DISCUSSION

Ionic gelation method is a technique used to synthesize CS-NPs via the electrostatic interaction between polycationic chains of CS in acidic media with negatively charged ions on TPP. This interaction occurs due to the cross linking of $NH_3$+ with phosphoric ions on TPP, as shown in Scheme 1 [23, 24].

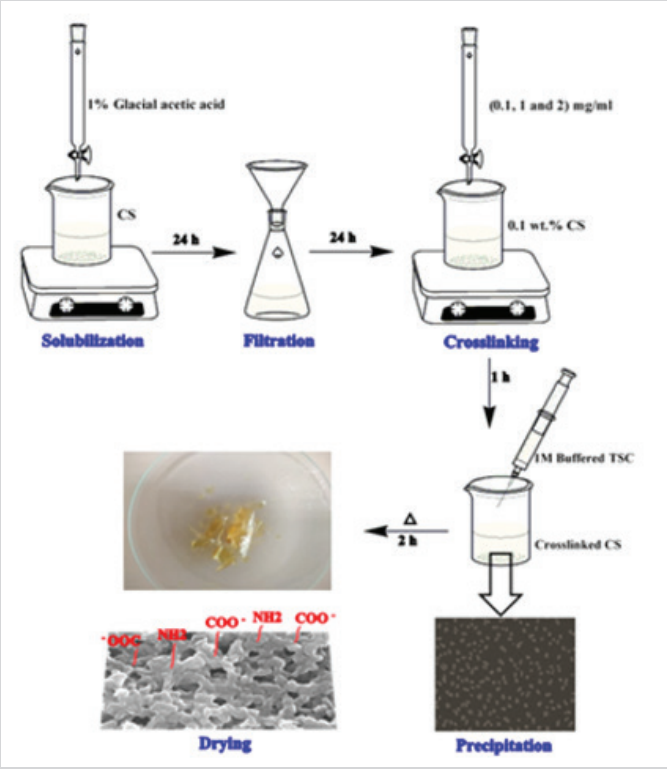


**Scheme 1:** A Schematic figure showing the method of CS-NPs synthesis.

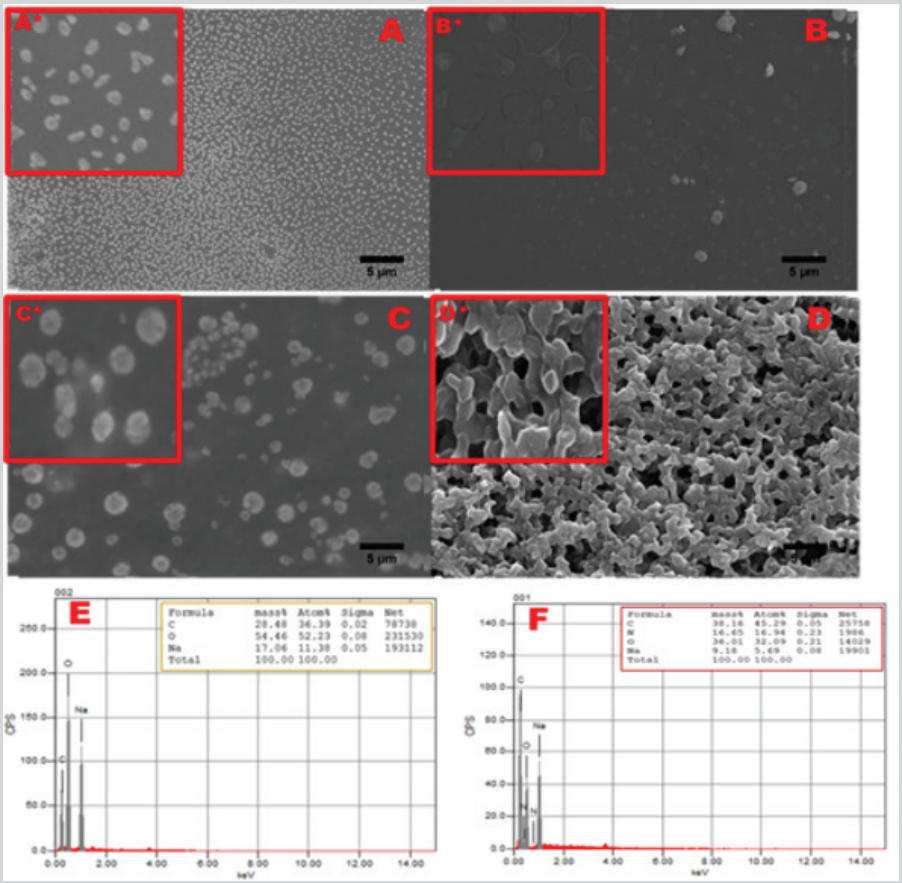


**Figure 1:** SEM micrographs for NCS (A) and (B) microporous CS and EDX analysis of free TSC (C) and microporous CS (D).

Figure 1 shows the SEM morphological characteristics of CS-NPs. It is apparent that, the synthesized CS-NPs exhibited an irregular shape at 0.1mg/ml of TPP concentration and a spherical shape with increasing TPP concentration. However, the interaction with TSC leads to a porous shape with new features that were investigated in this work. The interaction of polycationic chain in acidic media with negatively charged TPP ions leads to the formation of CS-NPs. This interaction occurs due to the cross linking of $NH_3$+ with phosphoric and OH- ions available in solution.

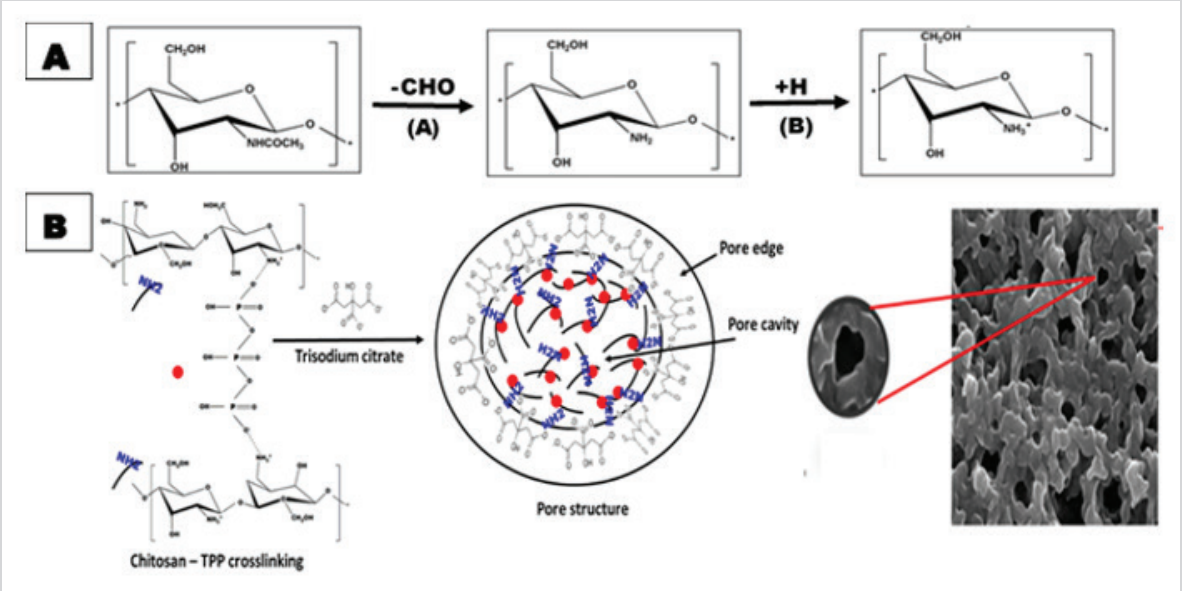


**Scheme 2:** A Schematic figure showing (A) Effect of solution pH on chitosan structure and scheme (B) A figure shows functionalization of chitosan with citrate and amine ions.

Also, CS has free amino groups ($NH_2$) that are formed at pH > 6 in a process called deacetylation process. The deacetylation process occurs due to the substitution of acetyl group (-CHO) with reactive amino group ($NH_2$) in alkaline media. At acidic pH < 6, the amino groups of chitosan capture H+ ions in solution and transforms into -$NH_3$+ in a process called protonation process. This process affects the chitosan chain depolymerization, deacetylation degree and so solubility. Thus, chitosan at pH > 6 tends to deprotonate -$NH_3$+ to neutral -$NH_2$ and tend to precipitate. This behavior means that the association forces dominate and the repulsive forces between particles are negligible. Trisodium citrate (TSC) is a crystalline salt whose buffer solution reaches pH of 6.2 (Scheme 2) [25]. Consequently, TSC ionically interacts with CS-NPs or CS-TPP through surface amine group and transforms into the porous morphology as observed in Figure 1. In this work, we performed further characterizations of the synthesized porous CS to investigate surface features including surface functionalization, porosity, and surface area.

**Table 2:** The effect of TPP concentration on the physiochemical properties of the synthesized CS-NPs.

| TPP Concentration | Hydrodynamic Size, (nm) | PDI | Zeta Potential, (+ mV) |
|---|---|---|---|
| 0.1mg/ml | 115.2nm | 0.285 | 55.44 ± 4.49 |
| 1mg/ml | 87.7nm | 0.386 | 39.63 ± 5.01 |
| 2mg/ml | 281.3nm | 0.31 | 34.15 ± 3.96 |

Table 2 reports the hydrodynamic size, zeta potential and PDI of different forms of synthesized CS-NPs. The smallest hydrodynamic size of ~87.7nm was obtained at TPP concentration of 1mg/mL and the lower PDI value of ~0.285 was obtained at TPP concentration of 0.1mg/ml. However, the highest zeta potential value was of ~+55.44mV, obtained at TPP concentration of 0.1mg/ml. Thus, it was concluded that size tends to decrease with elevation of TPP concentration until equals the CS concentration as more chitosan was crosslinked with more TPP molecules. However, size increases when TPP concentration exceeds CS concentration due to chitosan aggregates. This may be due to the open type of aggregation that occurs when aggregation and association forces overcome lower Coulombic repulsive forces between charged groups characterized with the lowest zeta potential value at higher pH [26].

## Characterization of Microporous CS

To investigate elemental analysis of the synthesized porous CS, we performed SEM - EDX, that detects elements within only a depth of 3μm. Figure 1E and 2F show the presence of C, O and Na peaks in free TSC sample while CS-TSC sample exhibited N peak in addition to the previous elements appears. Mass fractions of O and Na elements (wt%) in CS-TSC exhibited a decrease while C elements a slight increase than free TSC. Besides, the atomic fraction (at%) of C, N, O and Na is about 1:0.37:0.7:0.1 and 1:0:1.4:4.5 in CS-TSC and free TSC, respectively.

To investigate surface features of the synthesized porous CS, we used BET technique to determine surface area and pore volume/diameter. Figures 2 shows that CS after complexation with TSC as microporous material whose pore diameter is about 1.92nm and a large specific surface area of about 245.571$m^2$/g. Furthermore, pore volume reaches about 0.155$cm^3$/g with a wide pore size distribution and narrow slit- shaped pores.

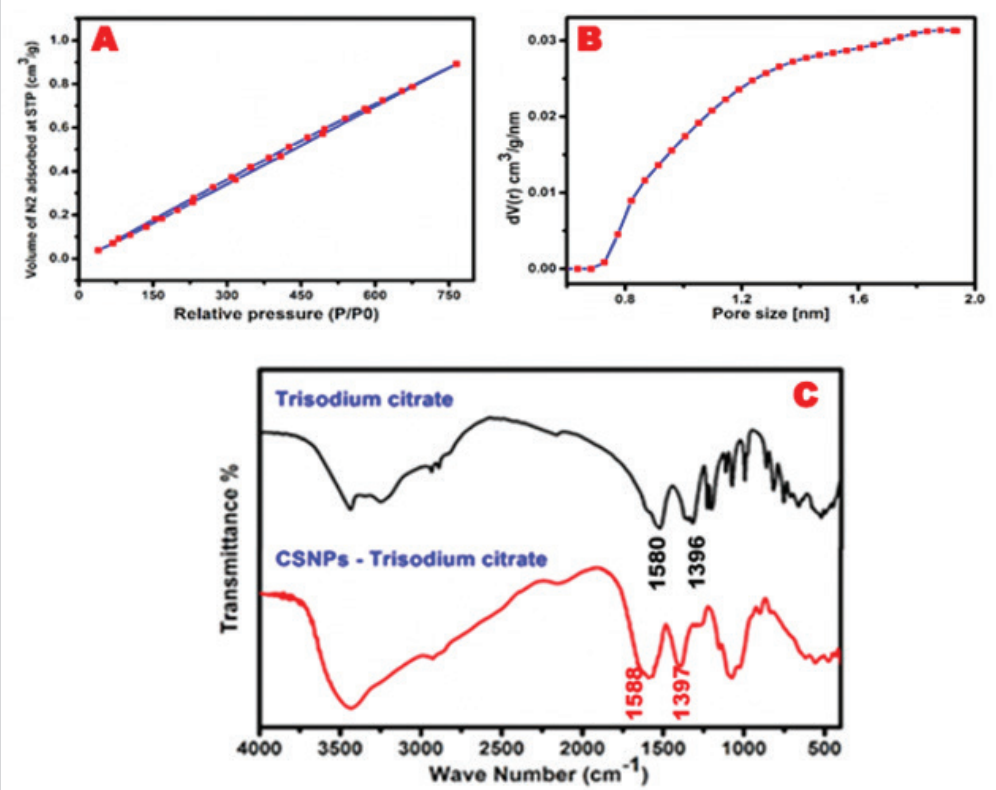


**Figure 2:** (A) Nitrogen absorption isotherm of microporous CS exhibited typical I curve with H4 hysteresis loop that gradually closed at a partial pressure near 0.4, (B) the corresponding pore size distribution using The BJH method and (C) FTIR spectra.

Besides, the surface functionalization of the microporous CS was studied using FT-IR technique. Figure 2 shows that the broad band at 300-3500cm-1 in both spectra is due to stretching of C-OH. The sharp band in TSC spectrum at 2924cm$^{-1}$ is due to C-H stretching vibration. The sharp bands at 1396 and 1580cm$^{-1}$ are due to the symmetric and anti-symmetric stretching of COO- as an indication of citrate ions. [27] However, the interaction of $NH_2$ groups of CS with citrate anions of TSC was observed in TSC-CS-NPs spectrum that showed a shift toward the higher wavenumber at 1397 and 1588cm$^{-1}$. Moreover, Thus, it was confirmed that the precipitation process increases surface functional groups of microporous CS as free amine groups and carboxy groups to which different ligands can bind in drug delivery purposes [28, 29].

Further investigation of the surface elemental analysis and distribution of the microporous CS was performed using EDX - line and mapping analysis. N indicates amine group ($NH_2$) while C and O indicate carboxyl or citrate ions (COO-). Figure 3 revealed the elemental analysis of C, N, O and Na elements along a surface line of about 18um lengths. It was found that the abundance of C, O elements, especially at pore edges as an indication of free citrate ions. Otherwise, the ratio of N atoms increased at the region between pore edges or the intermediate regions that indicates the presence of free $NH_2$ in these regions as shown in Figure 3. The corresponding EDX spectrum of line analysis showed atomic fractions of C, N, O and Na elements as follows; 48.83, 19.67, 26.34 and 5.16, respectively as observed in Figure 3.

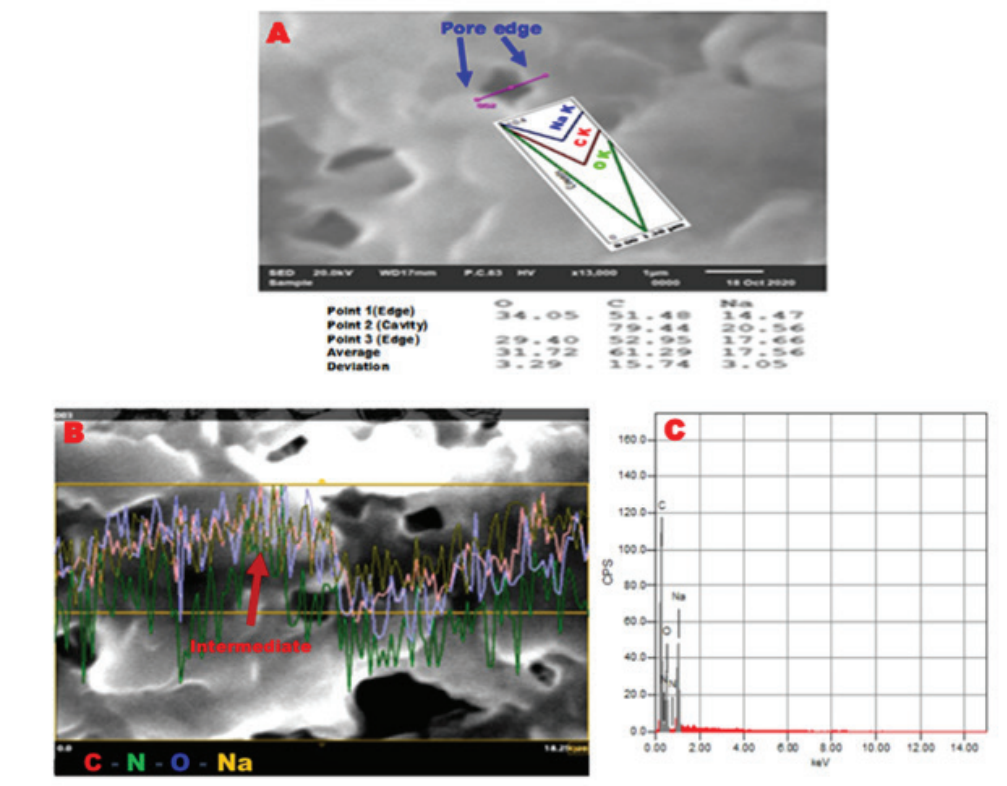


**Figure 3:** EDX-line analysis; (A) continuous line of about 18μm, (B) the corresponding elemental analysis and (C) triple point line of pore of microporous CS.

Figure 4 shows EDX - elemental maps of corresponding C, O, N and Na in the synthesized porous CS. Results confirmed that N concentration decreases than C and O at surface especially the intermediate regions than pore edges. It implies the contribution of $NH_2$ group of CS on hydrogen bonding with negatively charged COO- anions of TSC to resulted in the formation of this porous structure as shown in Scheme 2.

EDX results confirmed that pores edges are suspected to be formed of two layers, surface, and lower layers. The surface layer is mainly composed of citrate ions while the lower one is rich in amino groups. However, the intermediate portions between pores also includes surface amino groups in compared to edges. Consequently, it was revealed that the synthesized porous CS has functionalized with both citrate and amino groups that can act as protruding binding sites for various groups on drugs and ligands.

With regard to all previous results, CS-NPs synthesized with TPP concentration (0.1mg/mL) were the most suitable for protein loading purposes due to suitable size and narrow size distribution as well as higher stability degree that is reported in our previous work [21] to reach about three months in 4 °C and so they were used for *in vivo* study with BSA as a model of a protein involves some antigenic peptides in the sequence between 520-542aa [30].

## *In vivo* experiment

This experiment was carried out to investigate the toxicity of biocompatibility of the synthesized CS-NPs inside the body. male albino mice were IP injected with free and BSA-CS-NPs for nine days. blood and histopathological analysis were performed after three, six and nine days of administration.

## Clinical observation analysis

The total body weight and the relative weight of liver were investigated after three, six and nine days of IP administration of free and loaded CS-NPs. In general, Table 3 shows non-significant changes in all groups in compared to the negative control group.

Additionally, it was observed no mortality or behavioral changes in all treated groups with respect to the negative control mice.

Our results agree with the study by Aluni et al. [22] showed that CS/alginate nanoparticles did not change body weight, the relative weight of rat livers after repeated 14-day oral administration to rats. However, another study by Mehrabi et al. [31] reported that body weight in mice and guineapigs increases after the administration of three different doses of CSNPs and mannosylated CS nanoparticles during the seven-day period. In the other hand, no symptom of illness and death was observed during this period [31].

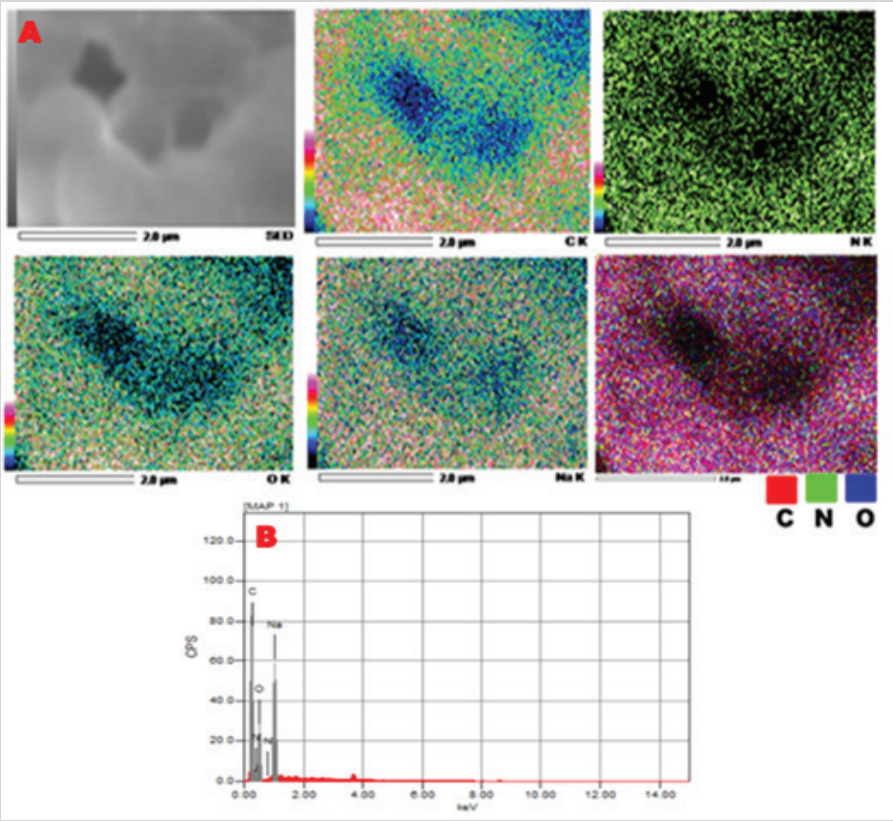


**Figure 4:** EDX - mapping analysis of microporous CS (A) and the corresponding elemental analysis (B).

## Biochemical analysis

Serum biochemical analysis was performed to determine the effect of free and loaded CS-NPs on the functionality of liver that can be indicated by alanine aminotransferase (ALT), aspartate aminotransferase (AST), albumin, globulin and Alb/Glb ratio. It was observed that no statistically significant changes in biochemical parameters in all groups in compared to the negative control group, as shown in Table 3.

**Table 3A:** The effect of CS-NPs and BSA-CS-NPs on body weight and relative weight of mice liver after three days of IP administration. Values are calculated as Mean ± SD (N = 3).

| Group | Body weight | Liver weight | AST | ALT | Alb | Glb | Alb / Glb |
|---|---|---|---|---|---|---|---|
| | (g) | (g) | (U/L) | (U/L) | (g/dl) | (g/dl) | |
| Negative control | 24.90 ± 2.39 | 0.072 ± 0.01 | 48.3 ± 30 | 57.6 ± 26.3 | 3.2 ± 0.5 | 1.2 ± 0.3 | 2.7 ± 0.7 |
| BSA control | 24.75 ± 2.27 | 0.068 ± 0.01 | 45 ± 25.1 | 57 ± 19.4 | 3.3 ± 0.6 | 0.86 ± 0.3 | 3 ± 1 |
| CS-NPs 1 control | 25.91 ± 2.26 | 0.071 ± 0.01 | 43 ± 28.3 | 56.6 ± 22.3 | 3.2 ± 0.5 | 1.4 ± 0.5 | 2.6 ± 0.9 |
| CS-NPs 2 control | 24.26 ± 4.54 | 0.085 ± 0.02 | 61.6 ± 8.6 | 46.3 ± 25 | 3.3 ± 0.2 | 1.2 ± 0.4 | 2.9 ± 0.7 |
| BSA-CS-NPs 1 | 27.72 ± 1.67 | 0.072 ± 0.01 | 64.6 ± 26.8 | 43 ± 7 | 3.1 ± 0.4 | 1.6 ± 0.3 | 2 ± 0.5 |
| BSA-CS-NPs 2 | 24.37 ± 2.89 | 0.067 ± 0.01 | 40 ± 6.4 | 34.3 ± 6.6 | 3.2 ± 0.2 | 1.2 ± 0.2 | 2.7 ± 0.4 |

**Table 3B:** The effect of CS-NPs and BSA-CS-NPs on body weight and relative weight of mice liver after six days of IP administration. Values are calculated as Mean ± SD (N = 3).

| Treatment | Body weight | Liver weight | AST | ALT | Alb | Glb | Alb / Glb |
|---|---|---|---|---|---|---|---|
| | (g) | (g) | U / L | U / L | g/dl) | (g/dl) | |
| Negative control | 23.18 ± 3.08 | 0.074 ± 0.01 | 58 ± 35 | 56 ± 30 | 3 ± 0.5 | 1.1 ± 0.3 | 2.7 ± 0.4 |
| BSA control | 25.42 ± 1.96 | 0.077 ± 0.01 | 66.6 ± 33.6 | 40 ± 21.1 | 2.9 ± 0.5 | 1.4 ± 0.6 | 2.1 ± 0.9 |
| CS-NPs 1 control | 27.32 ± 3.84 | 0.072 ± 0.01 | 48.6 ± 28.1 | 57.4 ± 15.1 | 3.2 ± 0.8 | 0.9 ± 0.1 | 3.5 ± 0.3 |
| CS-NPs 2 control | 25.03 ± 1.11 | 0.077 ± 0.01 | 60 ± 22.7 | 20 ± 13.5 | 3.2 ± 0.3 | 1.3 ± 0.3 | 2.5 ± 0.4 |
| BSA-CS-NPs 1 | 22.82 ± 2.85 | 0.082 ± 0.02 | 68.7 ± 9.7 | 23 ± 6.2 | 3 ± 0.4 | 1.2 ± 0.5 | 2.5 ± 0.6 |
| BSA-CS-NPs 2 | 21.23 ± 2.89 | 0.071 ± 0.01 | 65 ± 25 | 35 ± 30 | 3.1 ± 0.3 | 1.2 ± 0.2 | 2.4 ± 0.4 |

**Table 3C:** The effect of CS-NPs and BSA-CS-NPs on body weight and relative weight of mice liver after nine days of IP administration. Values are calculated as Mean ± SD (N = 3).

| Treatment | Body Weight | Liver Weight | AST | ALT | Alb | Glb | Alb / Glb |
|---|---|---|---|---|---|---|---|
| | (g) | (g) | U / L | U / L | g/dl) | (g/dl) | |
| Negative control | 26.23 ± 3.96 | 0.073 ± 0.01 | 59.6 ± 38.5 | 58.3 ± 25.7 | 3 ± 0.4 | 1.2 ± 0.6 | 2.8 ± 0.9 |
| BSA control | 26.62 ± 4.86 | 0.072 ± 0.01 | 97 ± 14.1 | 58 ± 21.2 | 3.4 ± 0.9 | 1.4 ± 0.1 | 2.4 ± 0.1 |
| CS-NPs 1 control | 23.62 ± 3.88 | 0.071 ± 0.01 | 48 ± 14.9 | 41.5 ± 15.1 | 3.1 ± 0.3 | 1.4 ± 0.3 | 2.2 ± 0.5 |
| CS-NPs 2 control | 24.45 ± 3.63 | 0.072 ± 0.02 | 72 ± 42 | 26 ± 13.5 | 3.3 ± 0.1 | 1.5 ± 0.7 | 2.2 ± 0.9 |
| BSA-CS-NPs 1 | 26.10 ± 2.92 | 0.075 ± 0.01 | 45 ± 14.1 | 36.3 ± 6.2 | 2.7 ± 0.5 | 1.4 ± 0.4 | 1.9 ± 0.5 |
| BSA-CS-NPs 2 | 22.90 ± 6.4 | 0.073 ± 0.01 | 77 ± 27.2 | 55 ± 30 | 3.2 ± 0.2 | 1.6 ± 0.4 | 2 ± 0.5 |

This agrees with a study found that rats fed on different types of CS at doses of 100 and 200mg/Kg. bw exhibited no significant changes of liver enzymes after 21 days of administration. Besides, CS significantly decreased the negative effect of the 2,3,7,8 tetrachlorodibenzo-p- dioxin (TCDD) when compared with those untreated with chitosan [32].

However, it was found that rats fed on CS for 6 weeks showed a significant decrease in normal liver function enzymes (ALT and AST) [33]. Also, another study showed that 1% chitin or CS enriched diet caused a significant increase in the total protein and albumin levels after 2 and 4 weeks; but the globulin and albumin: globulin ratio increased on week 4 as compared to controls [34].

## Histopathological and ultrastructural analysis

Normal hepatic architecture with healthy hepatocytes filled with clear glycogynated nuclei due to adolescence [35] and sinusoids in the negative control of mice were exhibited (Figure 5). BSA control group showed smooth architecture without collagen fibers and an activation of Kupffer cells, sinusoidal leukocytes, and endothelial cells with a limited degree of cytoplasmic disorganization in hepatocytes after six days followed by gradual regeneration (Figure 5).

Normal architecture was observed in CS-NPs 1 control mice with healthy hepatocytes, reduced observable collagen fibers and sinusoids as well as the presence of Kupffer cells and sinusoidal leukocytes (Figure 6). some limited changes were observed in CS-NPs 2 control group as a reduced observed collagen fibers and a mild degree of cytoplasmic disintegration of hepatocytes after six days followed a gradual regeneration at day nine of administration characterized with the presence of binucleate cells (Figure 6).

BSA-CS-NPs 1 group showed normal hepatocytes except after six days showed a mild degree of disorganization in compared to the control groups of mice (Figure 7). With respect to the control groups of mice, BSA-CS-NPs 2 group showed a relatively higher degree of cytoplasmic disintegration of hepatocytes after six days followed by the gradual regeneration of the normal tissue at day nine with the presence binucleate cells (Figure 7).

The presence of Kupffer cells is expected as these cells represent liver macrophages found inside the sinusoids with the presence of endothelial cells and leukocytes to perform their function in fragmentation of injected formulations and thus, activation of the immune response to immunogenic peptides in BSA [36,37]. In general, the limited changes observed didn't affect liver functionality that confirmed by biochemical analysis of liver enzymes and total protein profile. Also, there was no evidence of fibrosis, necrosis or chronic hepatic inflammation in all groups.

These results agree with findings showed that the histological analysis of liver in rats treated with CS/alginate nanoparticles for 7 days and shrimp CS for 21 days [22] exhibited no significant changes nor signs of necrosis, regeneration changes and cell replacement [32].

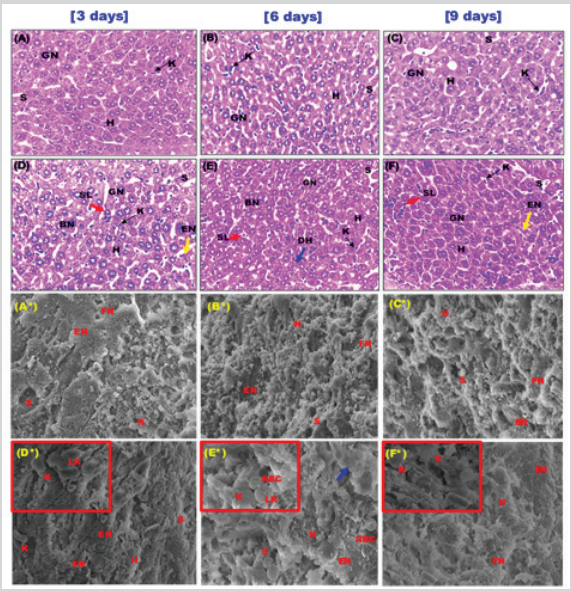


**Figure 5:** Photomicrographs of liver sections after three, six and nine days of administration; (A-C) the negative control group showed a normal hepatic architecture with healthy hepatocytes with clear glycogenated nuclei and sinusoids containing Kupffer cells, (D-F) BSA control group showed normal architecture with an activation of Kupffer cells, sinusoidal leukocytes and endothelial cells and a limited degree of disorganization in hepatocytes (blue arrow) after six days followed gradual regeneration of normal hepatocytes after nine days with the presence of binucleate cells (H&E stain, 400x). [scale bar = 40µm]; and SEM micrographs; (A*-C*) the negative control group showed intact liver ultrastructure without collagen fibers (2300X-Scale 10µm) and (D*-F*) BSA control group showed smooth architecture with the presence endothelial cells perforated with fenestrations and also a mild degree of disorganized hepatocytes (blue arrow) at six days of administration (2300X-Scale 10µm). (inset)- activated Kupffer cell and leukocytes present (6000X-Scale 2µm). hepatocytes (H), clear glycogenated nuclei (GN), sinusoids (S), Kupffer cells (K), endothelial cells (EN) and sinusoidal leukocytes (SL), leukocytes (LK) and fenestrations (FN).

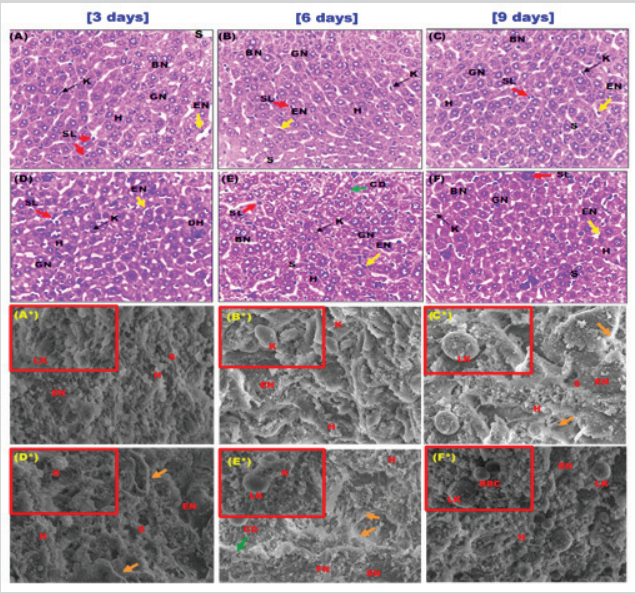


**Figure 6:** Photomicrographs of liver sections after three, six and nine days of administration; (A-C) CS-NPs 1 control group showed a normal hepatic architecture with an activation of Kupffer cells, sinusoidal leukocytes, and endothelial cells and binucleate cells. (D-F) CS-NPs 2 control group showed normal architecture with an activation of Kupffer cells, sinusoidal leukocytes and endothelial cells and a limited degree of cytoplasmic disintegration in hepatocytes (green arrow) after six days with the presence of binucleate cells (H&E stain, 400x). [scale bar = 40µm]; and SEM micrographs; (G-I) CS-NPs 1 control group showed normal ultrastructure with reduced collagen fibers (orange arrow) after nine days (2300X-Scale 10µm). (inset)- activated Kupffer cell and leukocytes present (6000X-Scale 2µm) and (J-L) CS-NPs 2 control group showed normal architecture with a reduced observable collagen fiber (orange arrow) and the presence endothelial cells perforated with fenestrations and also disorganized hepatocytes at six days of administration (2300X-Scale 10µm). (inset)- activated Kupffer cell and leukocytes present (6000X-Scale 2µm). hepatocytes (H), clear glycogenated nuclei (GN), sinusoids (S), Kupffer cells, endothelial cells (EN) and sinusoidal leukocytes (SL), leukocytes (LK) and fenestrations (FN).

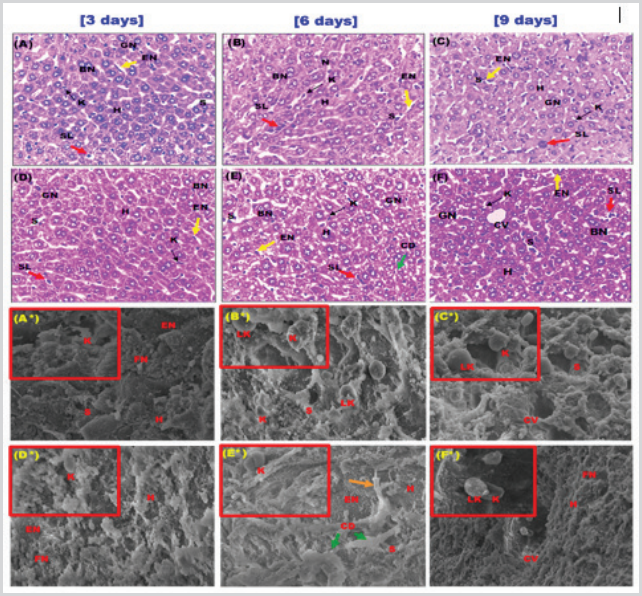


**Figure 7:** Photomicrographs of liver sections after three, six and nine days of administration; (A-C) BSA-CS-NPs 1 control group showed a normal hepatic architecture with an activation of Kupffer cells, sinusoidal leukocytes and endothelial cells and binucleate cells. (D-F) BSA- CS-NPs 2 treated group revealed normal hepatocytes and sinusoids containing Kupffer cells, endothelial cells and sinusoidal leukocytes. It was observed a higher degree of cytoplasmic disintegration in hepatocytes followed by a gradual regeneration of normal tissue as binucleate cells shown at 9 days. (H&E stain, 400x). [scale bar = 40µm]and SEM micrographs; (A*-C*) BSA-CS-NPs 1 control group showed normal ultrastructure with reduced collagen fibers (red arrows) after nine days (2300X-Scale 10µm). (inset)- activated Kupffer cell and leukocytes present (6000X-Scale 2µm) and (D*-F*) BSA-CS-NPs 2 control group showed normal architecture with a reduced observable collagen fiber (red arrows) and the presence endothelial cells perforated with fenestrations and also disorganized hepatocytes at six days of administration (2300X-Scale 10µm). (inset)- activated Kupffer cell and leukocytes present (6000X-Scale 2µm). hepatocytes (H), clear glycogenated nuclei (GN), sinusoids (S), Kupffer cells, endothelial cells (EN) and sinusoidal leukocytes (SL), leukocytes (LK) and fenestrations (FN).

## CONCLUSION

Herein, CS-NP was synthesized with different physiochemical characteristics and transformed into microporous CS using the ionic gelation method. The synthesized microporous CS chitosan have promising surface features relating to microporosity, large surface area and a suitable pore volume. Further, it has been functionalized with carboxyl and amino groups that will be helpful for drug delivery, antibacterial membranes and filters applications. Also, CS-NP with BSA as a model of carrier proteins was reported to be safe and biocompatible on the liver of mice with minor histopathological and ultrastructural alterations. Thus, this paper provides the reference for synthesis of safe CS-NPs that can be used in biomedical and pharmaceutical applications.

## AUTHORS CONTRIBUTION

Moataz Rashad: Performed experiments, analyzed data and wrote the paper. Maged El-Kemary: Designed and Supervised the research, co-wrote the paper, provided final approval of the version to publish and agreed to be accountable for all aspects of the work.

## FUNDING

This study did not receive any grant from any funding agency.

## COMPLIANCE WITH ETHICAL STANDARDS

This study was approved by the university human research ethics committee and all procedures performed in studies were in accordance with the ethical standards of the institutional and/or national research committee and with the 1964 Helsinki declaration and its later amendments or comparable ethical standards.

## REFERENCES

1. Shoueir KR, Desouky EN, Rasha MM, Ahmed MK, Janowska I, et al. (2020) Chitosan based nanoparticles and nanocapsules: Overview, physicochemical features, applications of a nanofibrous scaffold, and bioprinting. Intern J Biol Macromol 165: 1176-1197.
2. Rinaudo M (2006) Chitin and chitosan: Properties and applications. Prog Polym Sci 31(7): 603-632.
3. Shoueir K, Sheshtawy EH, Misbah M, Hosainy EH, Mehasseb EI, et al. (2018) Fenton-like nanocatalyst for photodegradation of methylene blue under visible light activated by hybrid green DNSA@ Chitosan@ MnFe2O4. Carbohydr Polym 197: 17-28.
4. Shoueir K, Kandil S, Hosainy EH, Kemary EM (2019) Tailoring the surface reactivity of plasmonic Au@ TiO2 photocatalyst bio-based chitosan fiber towards cleaner of harmful water pollutants under visible-light irradiation. J Clean Product 230: 383-393.
5. Polarz S, Smarsly B (2002) Nanoporous materials. J Nanosci Nanotechnol 2(6): 581-612.
6. Sami FEB, Mahfouz ME, Leporatti, S, Kemary ME, Hanafy AN (2019) Chitosan as a natural copolymer with unique properties for the development of hydrogels. Applied Sciences 9(11): 2193.
7. Riederer MS, Requist BD, Payne KA, Way JD, Krebs MD (2016) Injectable and microporous scaffold of densely packed, growth factor-encapsulating chitosan microgels. Carbohydr Polym 152:792-801.
8. Sudheesh K, Lakshmanan PT, Anilkumar VK, Ramya TV, Reshmi C, et al. (2012) Flexible and microporous chitosan hydrogel/nano ZnO composite bandages for wound dressing: in vitro and in vivo evaluation. ACS Appl Mater Interface 4(5): 2618-2629.
9. Lu Z, Gao J, He Q, Wu J, Liang D, et al. (2017) Enhanced antibacterial and wound healing activities of microporous chitosan-Ag/ZnO composite dressing. Carbohydr Polym 156: 460-469.

10. Kumar PS, Raj NM, Praveen G, Chennazhi KP, Nair SV et al. (2013) In vitro and in vivo evaluation of microporous chitosan hydrogel/nanofibrin composite bandage for skin tissue regeneration. Tissue Eng Part A 19(3-4): 380-392.

11. Mishra SK, Raveendran S, Ferreira JMF, Kanna S (2016) In situ impregnation of silver nanoclusters in microporous Chitosan-PEG membranes as an antibacterial and drug delivery percutaneous device. Langmuir 32(40): 10305-10316.

12. Yao J, Chen R, Wang K, Wang H (2013) Direct synthesis of zeolitic imidazolate framework 8/chitosan composites in chitosan hydrogels. Micropor Mesopor Mat 165: 200-204.

13. Verma D, Gulati N, Kaul S, Mukherjee S, Nagaich U (2018) Protein based nanostructures for drug delivery. J Pharm 2018.

14. Schepetkin IA, Plotnikov MB, Khlebnikov AI, Plotnikova TM, Quinn MT (2021) Oximes: Novel therapeutics with anticancer and anti-inflammatory potential. Biomolecules 11(6): 777.

15. Kardani K, Bolhassani A (2021) Antimicrobial/anticancer peptides: bioactive molecules and therapeutic agents. Immunotherapy 13(8): 669-684.

16. Patel DK, Dutta SD, Ganguly K, Cho SJ, Lim KT (2021) Mushroom-derived bioactive molecules as immunotherapeutic agents: A review. Molecules 26(5): 1359.

17. Singh S, Mishra P, Banga I, Parmar AS, Tripathi PP, et al. (2018) Chemiluminescence based immunoassay for the detection of heroin and its metabolites. BioImpacts: BI 8(1): 53-58.

18. Lin H, Hong H, Wang J, Li C, Zhou Z, et al. (2020) Rhamnose modified bovine serum albumin as a carrier protein promotes the immune response against sTn antigen. Chem Commun 56(90): 13959-13962.

19. Lu Z, Gao J, He Q, Wu J, Liang D, et al. (2017) Enhanced antibacterial and wound healing activities of microporous chitosan-Ag/ZnO composite dressing. Carbohydr Polym 156: 460-469.

20. Popova EV, Zorin IM, Domnina NS, Novikova II, Krasnobaeva IL (2020) Chitosan–Tripolyphosphate Nanoparticles: Synthesis by the Ionic Gelation Method, Properties, and Biological Activity. Russ J Gen Chem 90(7): 1304-1311.

21. Rashad MM, Kemary ENM, Amer S, Kemary EM (2021) Bovine serum albumin/chitosan-nanoparticle bio-complex; spectroscopic study and in vivo toxicological–Hypersensitivity evaluation. Spectrochim Acta A Mol Biomol Spectros 253: 119582.

22. Aluani D, Tzankova V, Kondeva BM, Yordanov Y, Nikolova E, et al. (2017) Evaluation of biocompatibility and antioxidant efficiency of chitosan-alginate nanoparticles loaded with quercetin. Int J Biol Macromol 103: 771-782.

23. Bagheri R, Ariaii P, Motamedzadegan A (2021) Characterization, antioxidant and antibacterial activities of chitosan nanoparticles loaded with nettle essential oil. J Food Meas Charact 15 (2): 1395-1402.

24. Pedroso SS, Fleitas SN (2020) Ionotropic gelation method in the synthesis of nanoparticles/microparticles for biomedical purposes. Polym Int 69(5): 443-447.

25. Bhumkar DR, Pokharkar VB (2006) Studies on effect of pH on cross-linking of chitosan with sodium tripolyphosphate: a technical note. AAPS Pharm Sci Tech 7(2) E138-E143.

26. Win KY, Feng SS (2005) Effects of particle size and surface coating on cellular uptake of polymeric nanoparticles for oral delivery of anticancer drugs. Biomaterials 26(15): 2713-2722.

27. Mohan JC, Praveen G, Chennazhi KP, Jayakumar R, Nair SV (2013) Functionalized gold nanoparticles for selective induction of in vitro apoptosis among human cancer cell lines. J Exp Nano Sci 8(1): 32-45.

28. Ji JG, Hao SL, Dong J, Zhang JF, Li JJ, et al. (2011) Preparation of chitosan/cyclodextrin/trisodium citrate nanoparticles for the poor-water drug carrier material. Adv Mat Res 152: 1356-1359.

29. Yao J, Chen R, Wan K, Wang H (2013) Direct synthesis of zeolitic imidazolate framework 8/chitosan composites in chitosan hydrogels. Micropor Mesopor Mat 165: 200-204.

30. Majorek KA, Porebski PJ, Dayal A, Zimmerman MD, Jablonska K, et al. (2012) Structural and immunologic characterization of bovine, horse and rabbit serum albumins. Mol Immunol 52(3-4): 174-182.

31. Mehrabi M, Dounighi NM, Rezayat SSM, Doroud D, Amani A, et al. (2018) Development and physicochemical, toxicity and immunogenicity assessments of recombinant hepatitis B surface antigen (rHBsAg) entrapped in chitosan and mannosylated chitosan nanoparticles: as a novel vaccine delivery system and adjuvant. Artif cells nanomed Biotechnol 46(Sup 1): 230-240.

32. Darwesh OM, Sultan YY, Seif MM, Marrez DA (2018) Bio-evaluation of crustacean and fungal nano-chitosan for applying as food ingredient. Toxicol Rep 5: 348-356.

33. Abdel KZM, Rahman AEMK, Hassan LE (2013) Chitosan as a hepato-protective agent against single oral dose of dioxin. IOSR J Environ Sci Toxicol Food Technol 7(3): 11-17.

34. Mari LSS, Jagruthi C, Anbazahan SM, Yogeshwari G, Thirumurugan R, et al. (2014) Protective effect of chitin and chitosan enriched diets on immunity and disease resistance in Cirrhina mrigala against Aphanomyces invadans. Fish & Shellfish Immunol 39(2): 378-385.

35. Geller SA, Petrovic LM (2004) Biopsy interpretation of the liver. Lippincott Williams & Wilkins, USA.

36. Kawada N, Parola M (2015) Interactions of stellate cells with other non-parenchymal cells. In Stellate cells in health and disease. Academic Press. Pp: 185-207.

37. Smith k (2013) Kupffer cells regulate the progression of ALD and NAFLD. Nature Reviews Gastroenterology & Hepatology 10(9): 503-503.